Rapid water parcel transport across the Kuroshio Extension in the lower thermocline from dissolved oxygen measurements by Seaglider

Shigeki Hosoda (hosodas@jamstec.go.jp)
Japan Marine-Earth Science and Technology https://orcid.org/0000-0002-3059-0027
Ryuichiro Inoue
JAMSTEC
Masami Nonaka
JAMSTEC
Hideharu Sasaki
JAMSTEC
Yoshikazu Sasai
JAMSTEC
Mizue Hirano
JAMSTEC

Research article

Keywords: Seaglider, small water parcels, water mass exchange, Kuroshio Extension, mesoscale eddy, submesoscale, dissolved oxygen

Posted Date: July 23rd, 2020

DOI: https://doi.org/10.21203/rs.3.rs-44183/v1

Version of Record: A version of this preprint was published on February 3rd, 2021. See the published version at https://doi.org/10.1186/s40645-021-00406-x.

Abstract

Small water parcels with low salinity and high dissolved oxygen (DO) are observed in the main thermocline south of the Kuroshio Extension (KE). The Seaglider data, which was collected for four months beginning in late winter 2014 with fine spatial and temporal resolutions, identified small water parcels characterized by low salinity and high DO in the subsurface layer (26.0–27.0 σ_θ) with a few ten kilometers and a few ten meters in the horizontal and vertical scales, respectively. Water mass analyses revealed larger negative salinity anomalies (< − 0.05 PSS-78) and positive DO anomalies (> 15 μmol kg^{-1}) than those of the surrounding water. The characteristics are similar to those of water mass with low salinity and high DO in the subpolar Northwestern Pacific Ocean. Additionally, higher DO anomaly water parcels appear in the upper layer (< 26.7 σ_θ) while low salinity parcels appear in the lower layer (> 26.7 σ_θ). Oxygen consumption rates from the apparent oxygen utility suggest that the small water parcels consume less oxygen than the surrounding water, implying that they migrate in a shorter time across the KE after subduction and their characteristics may reflect the sea surface temperature, salinity, and DO in the subduction region. Similar small water parcels represented by high-resolution numerical simulations indicate that they pass through the KE in one month. The simulations support the oxygen consumption rate from the Seaglider observations. The existence of a faster process for water mass migration by meso- and submesoscale subduction processes across the KE affects the amount, subduction, and exchange process of water mass. Our study indicates a small water mass contributes to the exchange process across the KE rapidly, which had not been identified in previous studies. Consequently, detailed observations using multiple Seagliders should capture detailed spatial and temporal variability of the water mass exchange process.

Introduction

Heat, freshwater, and material transports in the subsurface ocean play crucial roles in global climate change. As climate change evolves, they are being redistributed (e.g., Stocker 2013). In the western part of the ocean where a strong western boundary current exists, the water mass and materials are exchanged across the strong currents through a subduction process in the main thermocline (Marshall, 1997; Williams et al., 2001; Suga et al., 2008). This exchange significantly influences the climate system. In the North Pacific Ocean, the Kuroshio with a warm and saline water stream to the east, consists of the northwestern flank of the subtropical gyre, while the Oyashio with a higher dissolved oxygen (DO), cold and fresher water flows to the south along the east coast of Japan. These two major currents come in contact through the mixed water region (MWR), forming a strong meridional gradient of temperature and/or salinity front as the Kuroshio Extension (KE) (Talley et al., 1995; Yasuda et al., 1996).

The exchange process across the KE strongly affects both water mass modification and the dissipation of climate signals. A mechanism of water mass transformation across the KE has been suggested based on theories and observations (Marshall 1997; Williams et al., 2001; Spall 1995; Yoshikawa et al., 2001, 2012; Kouketsu et al., 2007; Inoue et al., 2016). Recently, high spatial density observations from the

shipboard conductivity, temperature-depth-oxygen profiler (shipboard CTD), and expendable conductivity-temperature-depth profiler (XCTD) (Yasuda et al 1996; Okuda et al 2001; Oka et al., 2009) found small water parcels with low potential vorticity (PV), high DO, and/or low salinity in the main thermocline around the MWR and KE. These results are supported by subsurface ocean mooring and BGC Argo float with DO sensors (Zhang et al., 2015; Nagano et al., 2016).

Nagano et al. (2016) observed variability in the temperature, salinity, and DO for 10 months at the south of the KE using temporal and fine resolution observations of mooring data. Seasonal and inter-seasonal variations were detected during the passage of mesoscale eddies and submesoscale water parcels with high DO and low salinity. They intermittently observed a high DO signal at 600 m. This was attributed to an elongated filament water mass of compressed subduction in the ageostrophic current across the KE flow with a detached cyclonic eddy from the meandering KE, although low salinity small water parcels without high DO and low PV existed. Hence, meso- and submesoscale phenomena strongly affect water originating from the Oyashio, which is subducted and comes across the KE.

Focused observational approaches using lots of Oxygen Argo floats successfully captured meso- and submesoscale phenomena in the anticyclonic eddy at the south of KE first (project name is “S1-INBOX”, which was carried out in 2011; Inoue et al., 2016). Zhang et al. (2015) observed sub-thermocline eddies with low salinity and high DO water using frequent measurements of Oxygen Argo floats in an anticyclonic eddy south of the KE in spring 2014. The daily profile data showed that the observed small water parcels all had low PV. However, the layer of 26.5–26.8 σ_θ exhibited contrary characteristics. Some layers had low temperature, low salinity, and high DO, but others had high temperature, high salinity, and low DO. They concluded that the size of the detected water parcels was 150–190 m in the vertical direction and about 20 km in the horizontal direction, resembling a thin lens moving at a horizontal speed of 10–15 cm s^{-1}.

Li et al. (2017) investigated the distribution and frequency of small water parcels in the Northwestern North Pacific Ocean using 337 profiles of Argo temperature and salinity. Statistically, the size of water parcels was equivalent to the submesoscale. The density surface was distributed over a wide range, and the 26.7 σ_θ isopycnal surface was separated by their characteristics of the Transition Mode water (TRMW) for the upper layer and the North Pacific Intermediate Water (NPIW) for the lower layer. The seasonality of the occurrence rate was larger in the spring when the subducted water from the north of the KE was dominant. They concluded that water parcels play an important role in the cross-frontal flow across the KE.

Previous studies have reported similar phenomena from various kinds of CTDO observations. Some studies reported that water parcels are the key for heat and freshwater transport in large-scale phenomena. For example, Zhang et al. (2017) showed that water mass exchange from small water parcels contributes 1/4 of the subduction rate in the Northwestern Pacific area based on a reanalyzed dataset. On the contrary, vertically fine resolution profile data does not always capture small water parcels in the same area (e.g., Sukigara et al., 2011). Due to insufficient temporal and spatial resolutions

and the difficulty detecting them, it is difficult to capture the actual shape and size. Additionally, the origin of small water parcels is unknown due to the variability in the characteristics. Furthermore, small water parcels are generally weak, making them difficult to detect from satellite observations. Consequently, subsurface ocean observations are necessary (Johnson and McTaggart, 2010; Bower et al.,2013).

Seaglider, which is an autonomous subsurface ocean observation tool, can measure the temperature, salinity, and DO from sea surface to 1000 dbar, diving more frequently than on-board CTD or other observation tools (Ericksen et al., 2001). Since target and observation missions can be controlled in real-time and operated over several months, Seaglider can perform long-term and quasi-stationary observations with a high spatial and temporal density compared to previous observation methods.

In this study, we focus on the detailed structures of small water parcels based on temporally and spatially frequent measurements by a Seaglider, including the DO data. Using multi-sensor measurements with DO and CTD, we suggest the relative age of small water parcels and qualitatively discuss the potential advection of a younger age water mass detected at the south of the KE in the subsurface layer.

The rest of this paper is organized as follows. First, we describe the data and method used. Second, the results of the Seaglider data analyses and the detailed characteristics of the water parcels are shown. Third, the possibility of detecting younger age water parcels in the main thermocline is considered by introducing the high-resolution Ocean general circulation model For the Earth Simulator (OFES) analyses. Finally, we summarize this study and future perspectives of studying water parcels on the water mass exchange and modification.

Method And Experimental

The Seaglider (manufactured by iRobot (now moved to Kongsberg), S/N: sg551) equipped with conductivity, temperature, pressure, and DO sensors was operated at the south of the KE (30–32.5°N, 143–145°E) where mesoscale eddies are frequently detached. In the late winter–early summer (February 27 to June 21, 2014), 693 vertical casts from the sea surface down to 1000 dbar were obtained (Figs. 1a and 2a). Only the downcast profiles were used because the downcast speed is more stable than the upcast speed. The stability of each profile affects the accuracy as well as temporal and horizontal sampling intervals. Table 1 shows the vertical sampling intervals. Each profile is vertically interpolated every 1 dbar using the Akima spline (Akima, 1970). Because the salinity and DO profiles at three stations were missed (dive no.: 131, 146, and 639), we filled these profiles with the linearly interpolated values using neighboring temporal profiles.

Table 1
Vertical sampling level of Seaglider.

Pressure (dbar)	Temp & Sal interval (dbar)	DO interval (dbar)
0-150	5	10
150–300	10	10
300–600	20	20
600–1000	30	30

The accuracy of the Seaglider data was verified using the shipboard CTD profiles at the launched point (Hakuho Maru KH14-1 cruise; February 27, 2014) and at the recovery point (Kaiyo KY14-9 cruise; June 21, 2014). Specifically, the presence of a salinity bias was verified. All Seaglider profiles were judged to have a sufficient accuracy for the analyses. The average time interval between profiles was 4.0 hours, and the average spatial interval was 2.3 km (Figs. 2b and 2c). The intervals were mostly uniform.

For simplicity when analyzing the characteristics of the water parcels, all the profiles were converted to the horizontal distance originating from the launching point. Anomalies in the temperature, salinity, and DO were calculated based on the differences from their average values through the observation periods by pressure level because the seasonal variation in the subsurface layer was below the detection limit for small water parcels. From the anomalies, the standard deviations were calculated for temperature, salinity, and DO. The results were used to evaluate extremely large positive or negative anomalies of each parameter.

We also used Argo float data to compare the characteristics and origin of small water parcels obtained from the Seaglider data. For comparison, data from each source were plotted as potential temperature–salinity diagrams. We used the delayed-mode QCed Argo float data from the Global Data Assembly Center (GDAC; Argo, 2000; Argo, 2020), which was observed during the formation of the deep winter mixed layer (January–April 2014 in the area of western North Pacific subtropical and subpolar regions: 25–45°N, 140–160°E). To indicate the position of the Seaglider, we used the sea surface height anomaly (SSHA) from geoid using the AVISO SSHA data, which was produced by binning and averaging monthly values on 0.25° grids. The data used here was from May 1, 2014 to trim the gridded data in 29.5–36.0°N, 139.0–149.0°E (Fig. 1a).

Furthermore, the daily mean averaging data from a hindcast numerical simulation (OFES) was used, which realized meso- and submesoscale oceanic structures with a realistic topography. The model, which is based on the Modular Ocean Model (MOM3), covered the entire North Pacific between 100°E to 70°W and 20°S to 68°N. The horizontal resolution was 1/30° and the 54 levels in the vertical cover the ocean from the surface to a realistic bottom topography (Masumoto et al., 2004; Sasaki et al., 2008). The 1/30° OFES simulation can partially resolve the submesoscales, especially in the middle and low latitudes (Qiu et al., 2014; Sasaki et al., 2014). Atmospheric forcing of the simulation is from the 6-hourly Japanese 25-year reanalysis with a 1° resolution (Onogi et al., 2007). A simple nitrogen-based Nutrient-Phytoplankton-

Zooplankton-Detritus (NPZD) pelagic ecosystem model (Oschlies, 2001) is included in the OFES simulation. The evolution of the biological tracer concentration is governed by advection–diffusion equations with source and sink terms. To estimate the dissolved oxygen concentration, the source and sink terms (Sasai et al., 2006; 2010). The change in the DO concentration is calculated by the change in the nitrate concentration due to the ecosystem dynamics and the air-sea exchange of oxygen at the sea surface. The variability in the biological fields did not induce feedback in the physical fields.

Results

During the observation period, seasonal thermocline, halocline, and subsurface oxygen maximum gradually formed in the upper mixed layer, separating the Subtropical Mode Water (STMW) from the sea surface (Figs. 3a–c). Although a small semidiurnal perturbation of the internal tidal wave appeared for all pressure levels on a nearly half a day cycle, the vertical pressure level and vertical gradient of the main thermocline were relatively stable. However, in the main thermocline at levels of 400–900 dbar, small perturbations were observed from late-April to mid-May. Because this study focused on the perturbations equivalent to small water mass parcels, our analysis highlighted the details in the small water parcels for a 9-day period from April 28 to May 6, 2014. During this period, the Seaglider was positioned around 31.7–32.8°N, 144.5–144.7°E, which was the southwestern side of an anticyclonic eddy and far west (over 250 km) of a cyclonic eddy detached from the KE (Fig. 1a). At the same time, the northwestward current velocity estimated by the Seaglider gradually increased and eventually reached around 40 cm s^{-1} (Fig. 1b).

During the highlighted period, small water parcels with temperature, salinity, and DO anomalies were observed below the winter mixed layer depth (MLD) along 26.0–27.0 σ_θ isopycnal surfaces (Figs. 4a–c), which almost corresponded to the density ranges of the North Pacific Central Mode Water (NPCMW; 26.2–26.4 σ_θ; Nakamura 1996; Suga et al., 1997) and the North Pacific Intermediate Water (NPIW; ~26.8 σ_θ; Talley et al., 1995). In the layer below the MLD, many anomalies in temperature, salinity, and DO were detected with values of < − 0.5 °C, − 0.05 PSS-78, and > 15 μmol kg^{-1}, respectively. The water parcel sizes varied significantly. The horizontal width ranged from a few kilometers to several ten kilometers, while the vertical thickness was mostly 0.01–0.5 σ_θ. Low (high) temperature anomalies corresponded with low (high) salinity anomalies.

The high (low) DO anomalies did not always correspond with the low (high) temperature and salinity anomalies. Hence, the water parcel characteristics demonstrate that subducted water has complicated water mass properties. For example, water parcels observed around 26.7–26.9 σ_θ at a distance of 830–850 km along the x-axis have properties of low/high temperature and salinity anomalies, but only low DO anomalies. On the other hand, water parcels around 26.4–26.9 σ_θ at a distance of 790–820 km have low/high temperature, salinity, and high/low DO anomalies.

Regarding planetary potential vorticity ($f\ \rho^{-1}\ d\rho\ dz^{-1}$, hereafter PV), the significance of the relationship between low PV and low temperature/salinity and high DO anomalies was unclear below the main thermocline. Thus, the water parcels originate from the north of the KE where high PV water is dominant (not shown here). Detecting a wide potential density range suggests that small water parcels may come from a broader area on the northern part of the KE, including levels of > 26.8 σ_θ surface, which are not in contact with the winter cooling atmosphere (e.g., Talley et al.,1995; Yasuda et al., 1996).

To clarify whether anomaly bias exists, Figs. 5a–c plot the appearance frequencies of temperature, salinity, and DO anomalies divided into three levels of upper (26.2–26.4 σ_θ), middle (26.45–26.6 σ_θ), and lower (26.7–26.8 σ_θ) layers, respectively. The frequency was counted from the interpolated data on the isopycnal surfaces every 0.01 kg m^{-3} for all profiles. The characteristics of the water parcels are likely biased with high DO, low temperature, and low salinity concentrations in the middle and lower levels. By contrast, such biases are not obvious in the upper layer. Especially in the middle layer, negative-ward/positive-ward salinity/DO anomalies exist over a broad range (− 0.38 to 0.15 PSS-78 / −21 to 68 μmol kg^{-1}), which also suggests that water parcels are subducted and transported from a broader range north of the KE. Additionally, the size of each water parcel varies; the water parcels with a minimum 5–10 km horizontal width and 30–100 dbar vertical thickness frequently appeared throughout the observation period. The detected spatial size based on the Seaglider's results means the Seaglider observation has a large potential to accurately measure the size of the water parcels even below the main thermocline using a fine vertical sampling rate.

Figure 6 shows a θ–S diagram of the Seaglider data throughout the whole observation period along with the Argo float data in the western North Pacific Ocean observed in 25–45°N, 140–160°E for January 1 – Aprirl 30, 2014 for comparison. Based on the θ–S relationship from the Argo float data, a wide range of water mass characteristics were observed (saltier/fresher side of the figure is the southern/northern part of the KE). The water mass characteristics obtained from the Seaglider were broadly detected and within the range of those from the Argo float data. Because the Seaglider collected data south of the KE in the subtropical region, the subtropical water mass characteristics were dominant and corresponded to the saltier side of the θ–S diagram (orange dots). To represent the water parcels with anomalous low salinity or high DO water, salinity and DO anomalies over three times of the standard deviations (3 σ) estimated from those average values through the observed period were highlighted. The characteristics of some water parcels (colored with over 3 σ of low salinity and/or high DO concentration variability) observed in 26.0–26.9 σ_θ were elongated toward the fresher side of the diagram (green dots), indicating that the water parcels may originate from the northern part of the KE (close to plots colored with green from Argo data). The lower salinity of the water parcels around 3–9 °C is significant (< 34.0 PSS-78), which is the level in the lower layer of the main thermocline.

Figure 7 shows the σθ–S diagram of the Seaglider data using the same color scheme as in Fig. 6. The water parcels along 26.2, 26.5, and 26.7 σ_θ displayed low salinity characteristics, corresponding to minimum salinity values of 33.8, 33.6, and 33.5, respectively. The low salinity properties extended along

the isopycnal surfaces, indicating that the small water parcels occasionally intrude at arbitral isopycnal surfaces. Figure 8 shows the σ_θ–DO diagram of the Seaglider data using the same color scheme as in Figs. 6 and 7. In 26.2–26.7 σ_θ isopycnal surfaces, the DO concentration was basically the same within 150–200 μmol kg^{-1}, while a high DO water over 200 μmol kg^{-1} was detected within the isopycnal surfaces, which had a maximum of 250 μmol kg^{-1}. However, a high DO water does not correspond well with the low salinity water shown in Figs. 7 and 8. In addition, the high DO value below 26.7 σ_θ was unclear, indicating that higher DO water tends to be distributed in the upper layer relative to the lower salinity water in the lower layer. Figures 7 and 8 indicate that the σ_θ level appearing in low salinity water differs slightly from that of high DO water, suggesting that the origin and characteristic of subducted water parcels at the sea surface north of the KE differ from each other.

Based on the in situ DO concentration, temperature, and salinity values, the apparent oxygen utility (AOU) and saturated oxygen concentration were calculated. Hence, the relative residence time of water parcels was estimated since subduction from the sea surface saturated the seawater with oxygen by contacting the atmosphere. Figure 9 shows σθ–AOU/Cs (a ratio of AOU and saturated oxygen concentration, Cs) diagram from the Seaglider data. Note that small water parcels with larger negative salinity anomalies and the positive DO anomalies were located below the euphotic zone (here we assume above 200 m). Here, a low AOU/Cs ratio means nearly saturated oxygen water, which occurs closer to the surface, while a high value of the ratio indicates far away from the sea surface. In other words, the ratio of water parcels positioned on the left side of the diagram indicates that less time has passed since the water parcels were on the sea surface. Assuming the water parcels move with time along a σ_θ surface after subduction, the relative age of a water parcel to the surrounding water mass can be estimated by comparing the AOU/Cs ratios. At a few σ_θ surfaces where water parcels with over 3 σ of DO and/or salinity anomalies were detected, AOU/Cs ratios of 0.18, 0.18, and 0.25 on 26.2–26.5 (26.7) σ_θ were observed, while those in the surrounding water were 0.3–0.4, 0.35–0.45, and 0.4–0.5, respectively. If the water parcels are advected with only some diffusive processes after subduction, then the water parcels with high DO and low salinity should be about 30–60% younger than the surrounding water on the same σ_θ, assuming that the water is unaffected by other processes to control the DO concentration. However, it is impossible to estimate the absolute age of a water parcel. Here, we discuss the age of water parcels as well as possibilities to detect younger water parcels using the high-resolution numerical model OFES.

Discussion

Based on the water mass analyses, we assumed that fresher and higher DO water parcels propagate across the KE from the northern part. How do these parcels arrive in the south KE below the main thermocline while maintaining low salinity and high DO properties? Here, we consider three possibilities to explain the DO concentration variation (Fig. 9). 1) Strong vertical mixing adds high DO and low salinity water during advection (e.g., Yoshikawa et al., 2002; 2012). 2) Oversaturated DO water is subducted below the sea surface and advects across the KE (e.g., Miyake and Saruhashi, 1966). 3) The water at the sea surface advects faster from the northern part of the KE. Since the water parcels were detected below

600 dbar and the higher DO concentrations were observed from those water characteristics, here we consider the hypothesis 3) is appropriate.

Regarding the possibility of item 3), we examined whether the water parcels propagate quickly across the KE without large losing properties using the output of the 1/30° fine-resolution OFES model. In the longitude-depth sections of the salinity snapshot on May 15, 2003 (Fig. 10, top-left panel), low salinity water parcels (< 33.8 PSS-78) appeared in 142–150°E and in 26.4–26.8 σ_θ. From the salinity maps on the isopycnal surfaces, the extremely low salinity water (< 33.6 PSS-78) off east Japan (38°N, 142°E) on April 5 expanded southeastward, drifting with the southward flow on the edge of the cyclonic mesoscale eddy around 34°N 146°E from April 15 to 25. On April 30, a thin elongated filament-like water parcel with a low salinity (< 33.7 PSS-78) expanded to the west around the south of the mesoscale eddy. The elongated filament was pulled by the neighboring anticyclonic eddy at the center of 33°N 143°E, arriving south of the eddy on May 10–15. The low salinity water parcels shown in the zonal section correspond to the low salinity filaments on the isopycnal salinity map on May 5.

Figure 11 shows a similar zonal section snapshot and isopycnal distribution of DO in the OFES for the shallower layer (26.4–26.6 σ_θ) than in the case of salinity. The higher DO water parcels (> 200 μmol kg^{-1}) appeared off east Japan around 37°N 143°E; then, they advected to the southeast like in the salinity map on around April 15. Finally, the high DO water parcels approached south of the anticyclonic eddy at 33°N 143°E to the west of the cyclonic eddy at 34°N 146°E. The high DO water parcels shown in the DO zonal section also correspond with high DO filaments elongated westward in the isopycnal map on May 15. Comparing Figs. 10 and 11 shows that the high DO and the low salinity filaments correspond well with those detected in the upper (600–800 dbar) and lower (700–900 dbar) layers, respectively.

This suggests that the properties of water parcels displayed in the OFES data correspond well with those in the Seaglider data. In addition, the horizontal snapshots of DO and salinity on 26.5 and 26.7 σ_θ indicate a rapid advection process from the subpolar region to the subtropical region across the KE, which is largely in association with mesoscale eddies. Surprisingly, the time passed from off northern Japan to the south of the KE is less than one month in the OFES analysis. Compared to previous studies, which assumed the subduction process occurs in a wider area, this is quite short. For similarly small water parcels observed just south of the KE from mooring data, Nagano et al. (2016) estimated its age as about a half year, which is also shorter than the water age based on the traditional subduction theory (Luyten et al., 1983).

As seen in Figs. 10 and 11, the salinity and DO concentrations at the sea surface are complexly distributed with meso- and submesoscale phenomena. The observed water mass characteristics of temperature, salinity, and DO anomalies in the subsurface layer with variable time and spatial scales shown in Fig. 4 may reflect the complex distribution of the water characteristics at the sea surface. Although the water parcels obtained by high-resolution OFES agree well with the origin and the propagation path qualitatively, considering the scales of the observed water parcels, the model resolution is insufficient to show detailed influences of the meso- and submesoscale processes. Besides, the

Seaglider measurement in this study is too sparse for both directions to detect the accurate size of the water parcels, especially the vertical resolution in the subsurface layer. Therefore, to investigate a more detailed mechanism and water characteristics with the biogeochemical process, analyses with finer temporal and spatial scales are required using Seaglider observations and finer resolution numerical models. Such investigations will clarify the characteristics and mechanisms of small water parcels and the exchange process across oceanic fronts shown by this study.

Summary And Conclusion

The Seaglider was operated south of the KE from late winter to early summer. It observed small water parcels with high DO and low salinity on 26.0–27.0 σ_θ during two weeks in the spring season. At the southwestern side of an anticyclonic eddy just south of the KE, small water parcels with variable spatial sizes were detected with spatial scales of several to a few tens of kilometers. The DO concentration of the water parcels was larger than 150 μmol kg^{-1} and the salinity was lower than 34.0 PSS-78. Although water parcels with a low salinity on 26.4–26.7σ_θ were detected without low PV, the high DO on 26.2 σ_θ was similar to the water parcels described in previous studies. Our water mass analysis using the θ–S diagram showed the water parcels observed by the Seaglider originated from the north and advected across the KE. The rates of low salinity and high DO water parcels depended on the depth. A high DO water tended to appear in the upper layer, whereas low salinity water was more often present in the lower layer. Based on DO and AOU analyses, the low salinity and high DO water are relatively younger by about 30–60% than the surrounding water in the subtropical region, assuming that the water is unaffected by other processes that control the DO concentration on the same σ_θ surfaces. These results successfully detect detailed characteristics of water parcels in the subsurface layer with finer spatial resolution observations.

Using a fine horizontal resolution numerical model, similar water parcels were detected in the main thermocline just south of the KE. The trace path of the water parcels originated from east Japan, indicating that the anomalies of salinity and DO depend on the density range and origin. Additionally, meso- and submesoscale phenomena associated with the mesoscale activity affect the advection from the north to the south of the KE. In other words, the water may be transported across the KE by mesoscale eddies in the main thermocline. To clarify the mechanism of advection and the amount of transportation, further observations and quantitative analyses using fine resolution observational and numerical models are crucial. Our study demonstrates that additional information about water mass exchange can be obtained using integrated physical and biogeochemical processes and quantifying the migration of the small water parcels in the western part of the Pacific basin.

Declarations

Seaglider: The Seaglider dataset is available from the corresponding author upon reasonable request, including profile and technical data. The data inventory is also available in the summary report of

Hakuho-Maru cruise (KH14-1; in Japanese) https://ocg.aori.u-tokyo.ac.jp/member/eoka/cruises/kh-14-1/report/KH-14-1report.pdf.

Argo float data: The Argo profile data, which was compared with the Seaglider data, is available from the GDAC sites described in detail: Argo (2019) Argo float data and metadata from Global Data Assembly Centre (Argo GDAC). SEANOE. https://doi.org/10.17882/42182.

High-resolution OFES: The 1/30° OFES simulation datasets analyzed during this study are not publicly available due to the huge size of the daily data but are available upon reasonable request.

AVISO SSHA: The dataset used to explain the background environment in this study is available in the AVISO SSHA https://climatedataguide.ucar.edu/climate-data/aviso-satellite-derived-sea-surface-height-above-geoid.

Shipboard CTD cast: The CTD cast data of Hakuho-Maru cruise (KH14-1) and Kaiyo (KY14-9) for the Seaglider data calibration are available as inventories in

https://ocg.aori.u-tokyo.ac.jp/member/eoka/cruises/kh-14-1/report/KH-14-1report.pdf.

and

http://www.godac.jamstec.go.jp/catalog/doc_catalog/metadataDisp/KY14-09_all?lang=en, respectively.

Competing interests

The authors declare that they have no competing interests.

Funding

This work was supported by the Japan Society of Promotion of Science (JSPS) through Grants-in-Aid for Scientific Research in Innovative Areas 2205 and the Ministry of Education, Culture, Sports, Science and Technology (MEXT) of Japan through a Grant-in-Aid for Scientific Research on Innovative Areas (19H05700).

Authors’ contributions

SH proposed the topic, conceived, and designed the study. RI organized the Seaglider observations and collaborated in the study. MN conducted the experimental analysis using high-resolution OFES. HS created the high-resolution OFES data and supported the analysis. YS organized the NPZDC model for the OFES and supported the analyses. MH supported the Seaglider observations and resolved hardware issues regarding the operation. All authors read and approved the final manuscript.

Acknowledgments

We are grateful M. Hirano, Dr. K. Toyama, and Dr. K. Sato for their support of the Seaglider operations and JAMSTEC's Argo data management team for observations and data management. Regarding the deployment and recovery of the Seaglider, we thank Dr. K. Kutsuwada and Dr. Y. Kawai as the principal investigators and the crews of the Hakuho-Maru (KH14-1) and Kaiyo (KY14-9) for their great efforts in planning and implement the observations. The high-resolution OFES dataset was conducted using the Earth Simulator with the support of JAMSTEC. We thank the National Center for Atmospheric Research Staff (Eds) for their assistance in obtaining the sea surface height anomalies. Last modified July 1, 2016. "The Climate Data Guide: AVISO: Satellite-derived Sea Surface Height above Geoid." Retrieved from https://climatedataguide.ucar.edu/climate-data/aviso-satellite-derived-sea-surface-height-above-geoid. "The Argo float data were collected and made freely available by the International Argo Program and the national programs that contribute to it. (http://www.argo.ucsd.edu, http://argo.jcommops.org). The Argo Program is part of the Global Ocean Observing System."

This work was supported by the Japan Society of Promotion of Science (JSPS) through Grants-in-Aid for Scientific Research in Innovative Areas 2205 and the Ministry of Education, Culture, Sports, Science and Technology (MEXT) of Japan through a Grant-in-Aid for Scientific Research on Innovative Areas (19H05700).

Abbreviations

AOU: Apparent Oxygen Utility; BGC: Biogeochemical; CTD: Conductivity Temperature Depth device; DO: dissolved oxygen, GDAC: Global Argo data assembly center; KE: Kuroshio Extension; MLD Mixed layer depth; MOM: Modular Ocean Model; MWR mixed water region; NPCMW: North Pacific Central Mode Water; NPIW: North Pacific Intermediate Water; NPZD: Nutrient-Phytoplankton-Zooplankton-Detritus; PV: Potential Vorticity; SSHA: Sea surface height anomaly; STMW: Subtropical Mode Water; OFES: Ocean general circulation model For the Earth Simulator; TRMW: Transition Mode Water

References

1. Akima H (1970) A new method for interpolation and smooth curve fitting based on local procedures. J Assoc Comput Mech 17:589–603
2. Argo float data and metadata from Global Data Assembly Centre (Argo GDAC) https://doi.org/10.17882/42182
   Argo (2000) Argo float data and metadata from Global Data Assembly Centre (Argo GDAC). SEANOE. https://doi.org/10.17882/42182
3. Argo float data and metadata from Global Data Assembly Centre (Argo GDAC) https://doi.org/10.17882/42182

Argo (2019) Argo float data and metadata from Global Data Assembly Centre (Argo GDAC). SEANOE. https://doi.org/10.17882/42182

4. JAMSTEC (2009) JAMSTEC OFES (Ocean General Circulation Model for the Earth Simulator) Dataset. JAMSTEC. doi:10.17596/0002029 (accessed YYYY-MM-DD)
5. Bower AS, Hendry RM, Amrhein DE, Lilly JM (2013) Direct observations of formation and propagation of subpolar eddies into the subtropical North Atlantic. Deep Sea Res Part II 85:15–41. doi:10.1016/j.dsr2.2012.07.029
6. Eriksen CC, Osse TJ, Light RD, Wen T, Lehman TW, Sabin PL, Ballard JW, Chiodi AM (2001) Seaglider: A Long-Range Autonomous Underwater Vehicle for Oceanographic Research. IEEE JOURNAL OF OCEANIC ENGINEERING 26(4):424–436
7. Inoue R, Suga T, Kouketsu S, Kita T, Hosoda S, Kobayashi T, Sato K, Nakajima H, Kawano T (2016) Western North Pacific Integrated Physical-Biogeochemical Ocean Observation Experiment (INBOX): Part 1. Specifications and chronology of the S1-INBOX floats. J Mar Res 74(2):43–69
8. Inoue R, Faure V, Kouketsu S (2016) Float observations of an anticyclonic eddy off Hokkaido. J Geophys Res Oceans 121:6103–6120. doi:10.1002/2016JC011698
9. Johnson GC, McTaggart KE (2010) Equatorial Pacific 13 °C Water eddies in the eastern subtropical South Pacific Ocean. J Phys Oceanogr 40:226–236
10. Kouketsu S, Yasuda I, Hiroe Y (2007) Three-Dimensional Structure of Frontal Waves and Associated Salinity Minimum Formation along the Kuroshio Extension. J Phys Oceanogr. 37. DOI:10.1175/JPO3026.1
11. Li C, Zhang Z, Zhao W, Tian J (2017) A statistical study on the subthermocline submesoscale eddies in the northwestern Pacific Ocean based on Argo data. J Geophys Res Oceans 122:3586–3598. doi:10.1002/2016JC012561
12. Luyten JR, Pedlosky J, Stommel H (1983) The ventilated thermocline. J Phys Oceanogr 13:292–309
13. Masumoto Y et al (2004) A fifty-year eddy-resolving simulation of the World Ocean: preliminary outcomes of OFES (OGCM for the Earth Simulator). J Earth Simul 1:35–56
14. Marshall D (1997) Subduction of water masses in an eddying ocean. J Mar Res 55:201–222
15. Miyake Y, Saruhashi K (1966) On the radio-carbon age of the ocean waters. Pap Met Geophys 17:218–223
16. Nagano A, Suga T, Kawai Y, Wakita M, Uehara K, Taniguchi K (2016) Ventilation revealed by the observation of dissolved oxygen concentration south of the Kuroshio Extension during 2012–2013. J Oceanogr 72:837–850. DOI:10.1007/s10872-016-0386-9
17. Nakamura H (1996) A pycnostad on the bottom of the ventilated portion in the central subtropical North Pacific: its distribution and formation. J Oceanogr 52:171–188
18. Okuda K, Yasuda I, Hiroe Y, Shimizu Y (2001) Structure of Subsurface Intrusion of the Oyashio Water into the Kuroshio Extension and Formation Process of the North Pacific Intermediate Water. J Oceanogr 57:121–140

19. Oka E, Toyama K, Suga T (2009) Subduction of North Pacific central mode water associated with subsurface mesoscale eddy. Geophys Research Lett 36:L08607. doi:10.1029/2009GL037540
20. Onogi K et al (2007) The jra-25 reanalysis. J Met Soc Jpn 85:369–432
21. Oschlies A (2001) Model-derived estimates of new production: newresults point towards lower values. Deep-Sea Res II 48:2173–2197
22. Qiu B, Chen S, Klein P, Sasaki H, Sasai Y (2014) Seasonal mesoscale and submesoscale eddy variability along the North Pacific Subtropical Countercurrent. J Phys Oceanogr 44:3079–3098
23. Sasai Y, Ishida A, Sasaki H, Kawahara S, Uehara H, Yamanaka Y (2006) A global eddy-resolving coupled physical and biologicalmodel: physical influences on a marine ecosystem in the North Pacific. Simulation 82:467–474
24. Sasai Y, Richards K, Ishida A, Sasaki H (2010) Effects of cyclonic mesoscale eddies on the marine ecosystem in the Kuroshio Extension region using an eddy-resolving coupled physical-biological model. Ocean Dyn 60:693–704. doi:10.1007/s10236-010-0264-8
25. Sasaki H, Nonaka M, Masumoto Y, Sasai Y, Uehara H, Sakuma H (2008) An eddy-resolving hindcast simulation of the quasiglobal ocean from 1950 to 2003 on the Earth Simulator. In *High Resolution Numerical Modelling of the Atmosphere and Ocean*, K. Hamilton and W. Ohfuchi (eds.), Chap. 10, pp. 157–185, Springer, New York
26. Sasaki H, Klein P, Qiu B, Sasai Y (2014) Impact of oceanic-scale interactions on the seasonal modulation of ocean dynamics by the atmosphere. Nature Comm 5:5636-
27. Sukigara C, Suga T, Saino T, Toyama K, Yanagimoto D, Hanawa K, Shikama N (2011) Biogeochemical evidence of large diapycnal diffusivity associatedwith the subtropical mode water of the North Pacific. J Oceanogr 67:77–85. DOI 10.1007/s10872-011-0008-5
28. Stocker TF in Ocean Circulation and Climate (eds. Siedler, G. et. Al.) Ch.1 (International Geophysics Vol. 103, Academic Prewss, 2013)
29. Spall MA (1995) Frontogenesis, subduction, and cross-front exchange at upper ocean fronts. J Geophys Res 100(C2):2543–2557
30. Suga T, Aoki Y, Saito H, Hanawa K (2008) Ventilation of the North Pacific subtropical pycnocline and mode water formation. Prog Oceanogr 77:285–297. doi:10.1016/j.pocean.2006.12.005
31. Suga T, Takei Y, Hanawa K (1997) Thermostad distribution in the North Pacific subtropical gyre: The central mode water and the subtropical mode water. J Phys Oceanogr 27:140–152
32. Talley L, Nagata Y, Fujimura M, Kono T, Inagake D, Hirai M, Okuda K (1995) North Pacific intermediate water in the Kuroshio/Oyashio mixed water region. J Phys Oceanogr 25:475–501
33. Williams RG (2001) Ocean subduction. Encyclopedia of Ocean Sciences, Steele JH, Turekian KK and Thorpe SA Ed., Academic Press, 1982–1993
34. Yasuda I, Okuda K, Shimizu Y (1996) Distribution and modification of North Pacific Intermediate Water in the Kuroshio-Oyashio interfrontal zone. J Phys Oceanogr 26:448–465

35. Yoshikawa Y, Akitomo K, Awaji T (2001) Formation process of intermediate water in baroclinic current under cooling. J Geophys Res 106(C1):1033–1051
36. Yoshikawa Y, Lee CM, Thomas LN (2012) The Subpolar Front of the Japan/East Sea. Part III: Competing Roles of Frontal Dynamics and Atmospheric Forcing in Driving Ageostrophic Vertical Circulation and Subduction. J Phys Oceanogr 42:991–1011. doi:10.1175/JPO-D-11-0154.1
37. Zhang Z, Li P, Xu L, Li C, Zhao W, Tian J, Qu T (2015) Subthermocline eddies observed by rapid-sampling Argo floats in the subtropical northwestern Pacific Ocean in Spring 2014. Geophys Res Lett 42. doi:10.1002/2015GL064601
38. Zhang Z, Zhang Y, Wang W (2017) Three-component structure of subsurface-intensified mesoscale eddies in the ocean. J Geophys Res 122:1653–1664. doi:10.1002/2016JC012376

Figures

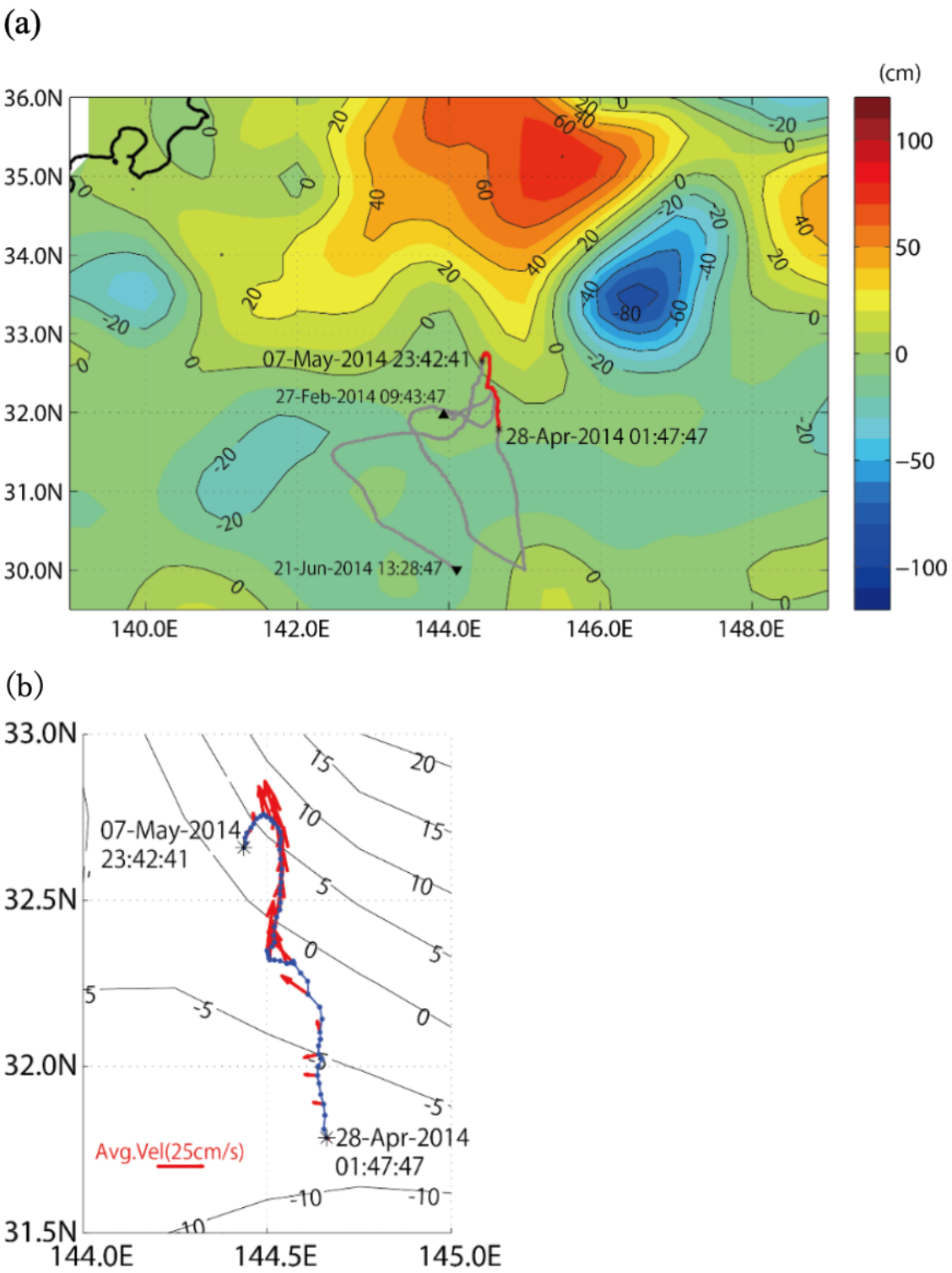

Figure 1

(a) Trajectory of Seaglider for Feb.27- Jun.21 (gray line between triangle at the deployed point and inverted triangle at the recovery point). Focused period on this study in Apr.28 – May 6 are highlighted (red line between black asterisks). Background color and contour lines display mean sea level height anomaly (SLHA; cm) during May 1-7. (b) Enlarged SSHA map of (a) with vertical averaged horizontal current velocity (cm s-1; red arrow plotted every third profile).

(a)

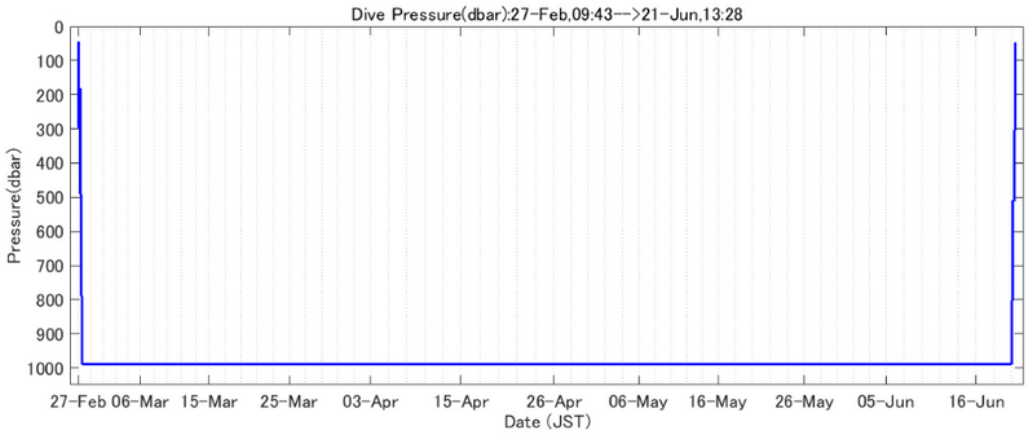

(b)

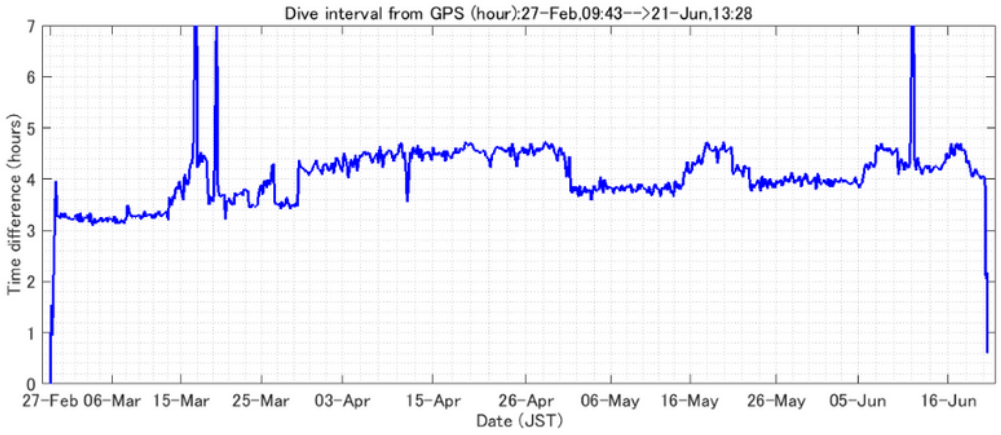

(c)

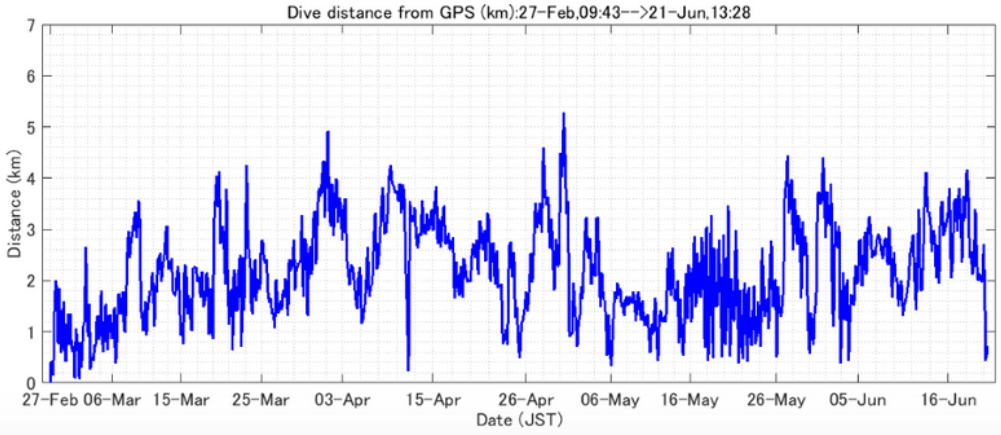

Figure 2

(a) Dive pressure for each cast (dbar), (b) time interval for each cast (hour), and (c) distance between each cast (km) through all Seaglider observation. Position, time and pressure are measured at downward cast.

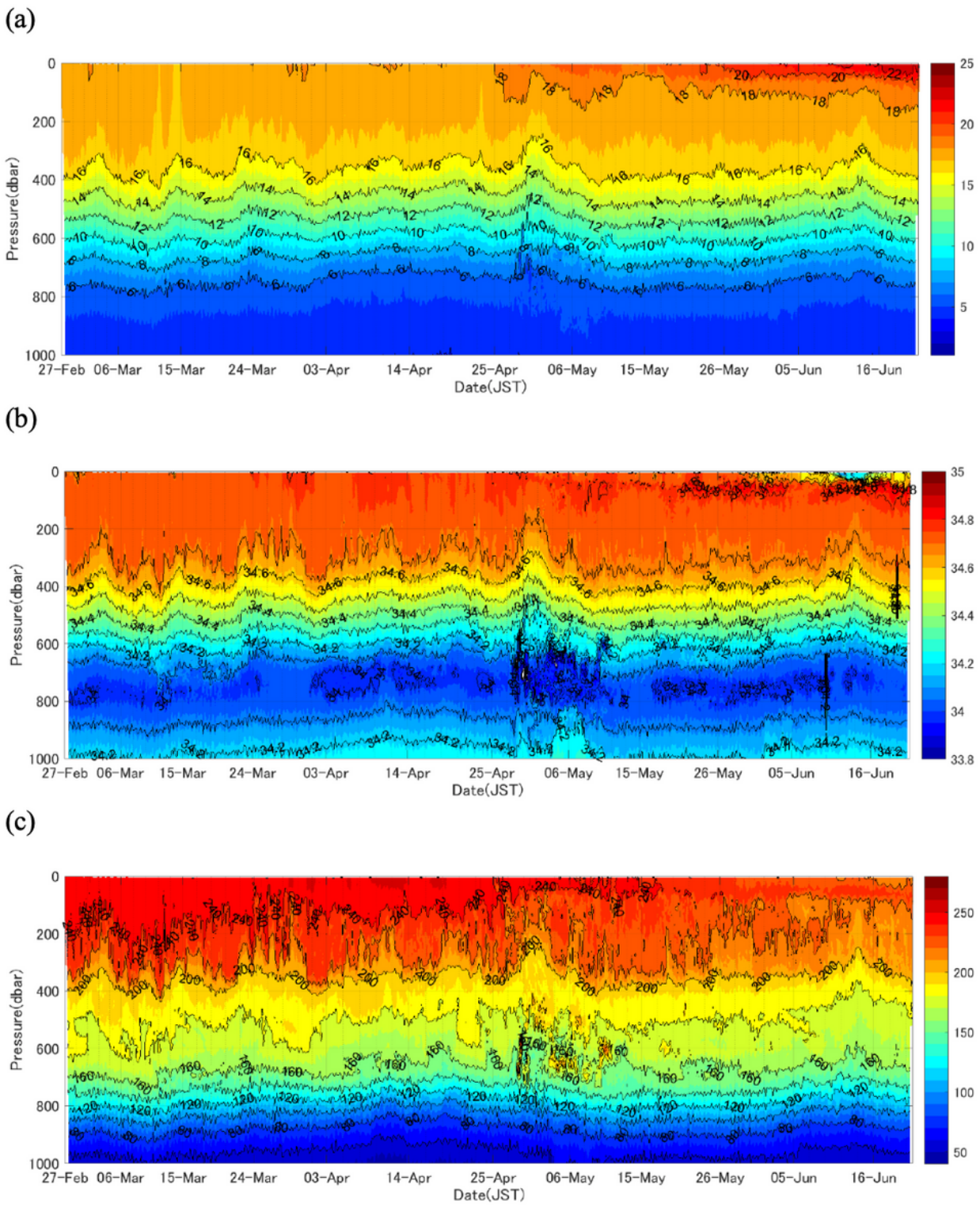

Figure 3

Time series of temperature (°C) (a), salinity (PSS-78) (b), and dissolved oxygen (DO) (μmol kg-1) (c) during whole observation (Feb.27- Jun.21, 2014). Contour intervals of temperature, salinity and DO concentration are 1 °C, 0.2 PSS-78 and 20 μmol kg-1, respectively.

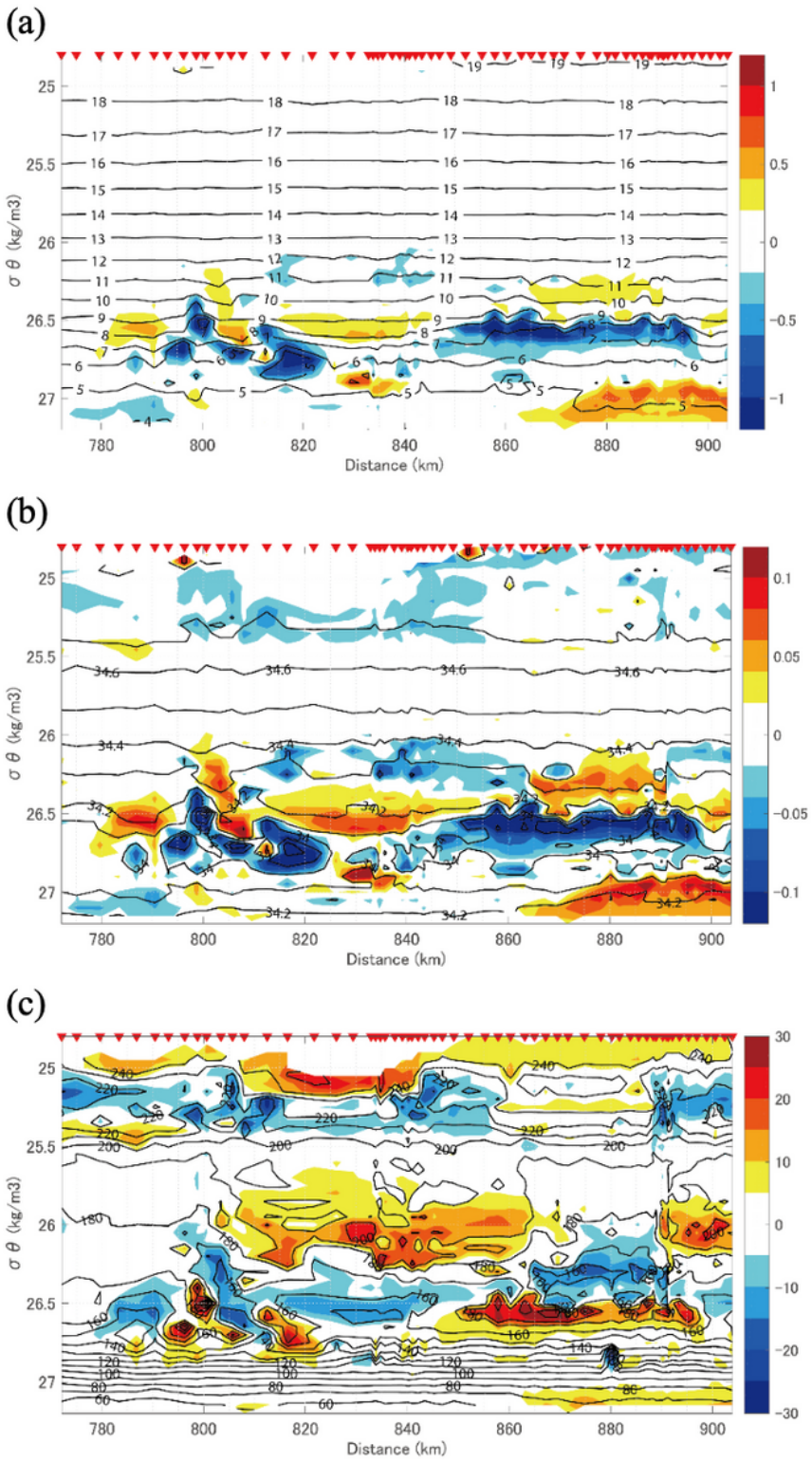

Figure 4

Time series of temperature (°C) (a), salinity (PSS-78) (b), and DO anomaly (μmol kg-1; contour) (c) on isopycnal surfaces during Apr. 28th – May 7th, with salinity and DO anomalies (color) calculated from average profiles through whole observed periods. Contour intervals of temperature, salinity and DO are 1°C, 0.1 PSS-78 and 20μmol kg-1 respectively. Those values on isopycnal surfaces are interpolated every 0.01 kg-1 m3 from the individual profiles of Seaglider data. Linear trends calculated from whole observed

period are removed for each parameter. X-Axis represent cumulative distances based on the launching point.

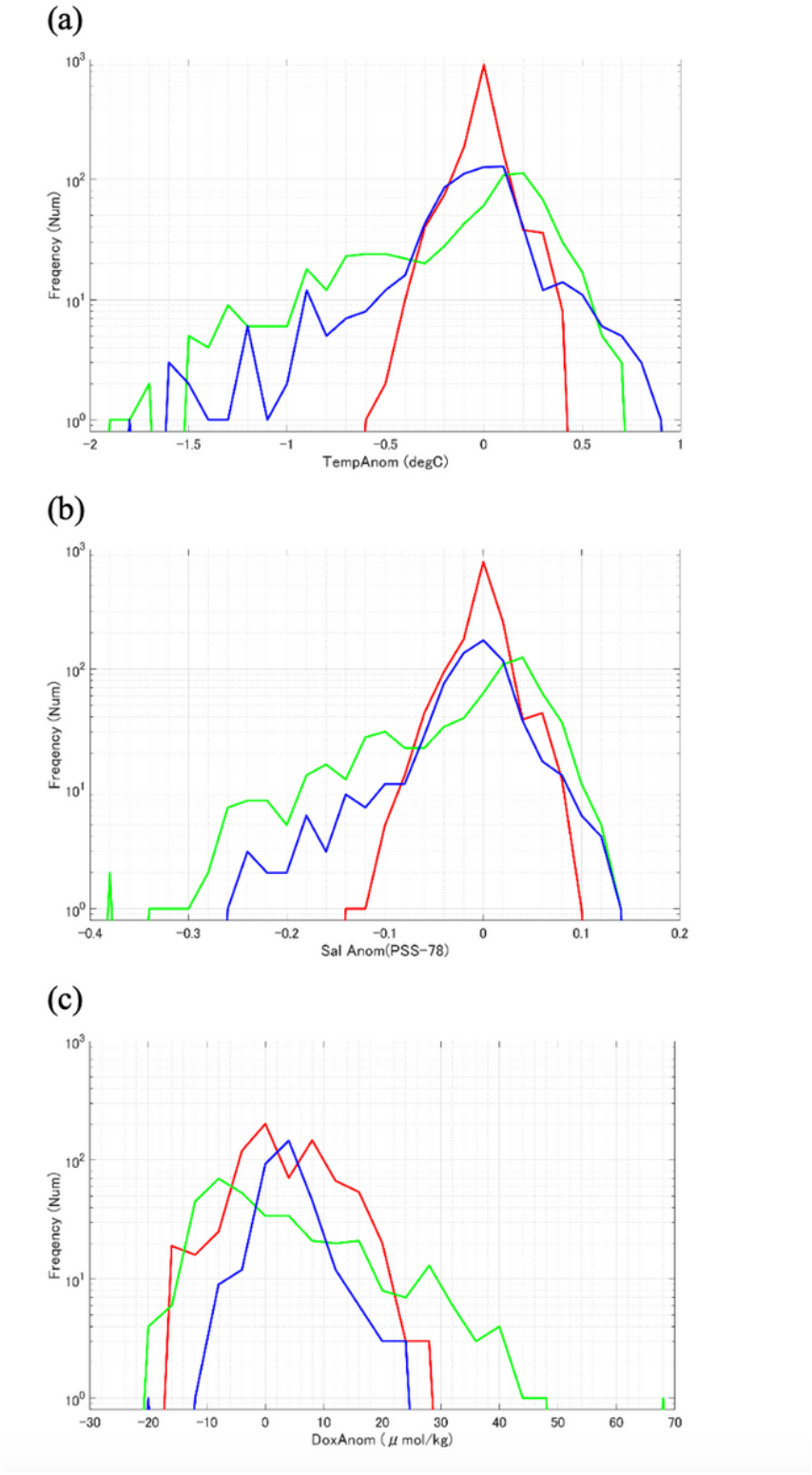

Figure 5

Frequency of temperature anomaly (a), salinity anomaly (b), and DO anomaly (c) on upper (red, 26.2-26.4σθ), middle (green,26.45-26.6σθ) and lower (blue, 26.7-26.8σθ) isopycnal layers. Frequency is counted based on 1km horizontally gridded data. Frequency below 100 equal zero count.

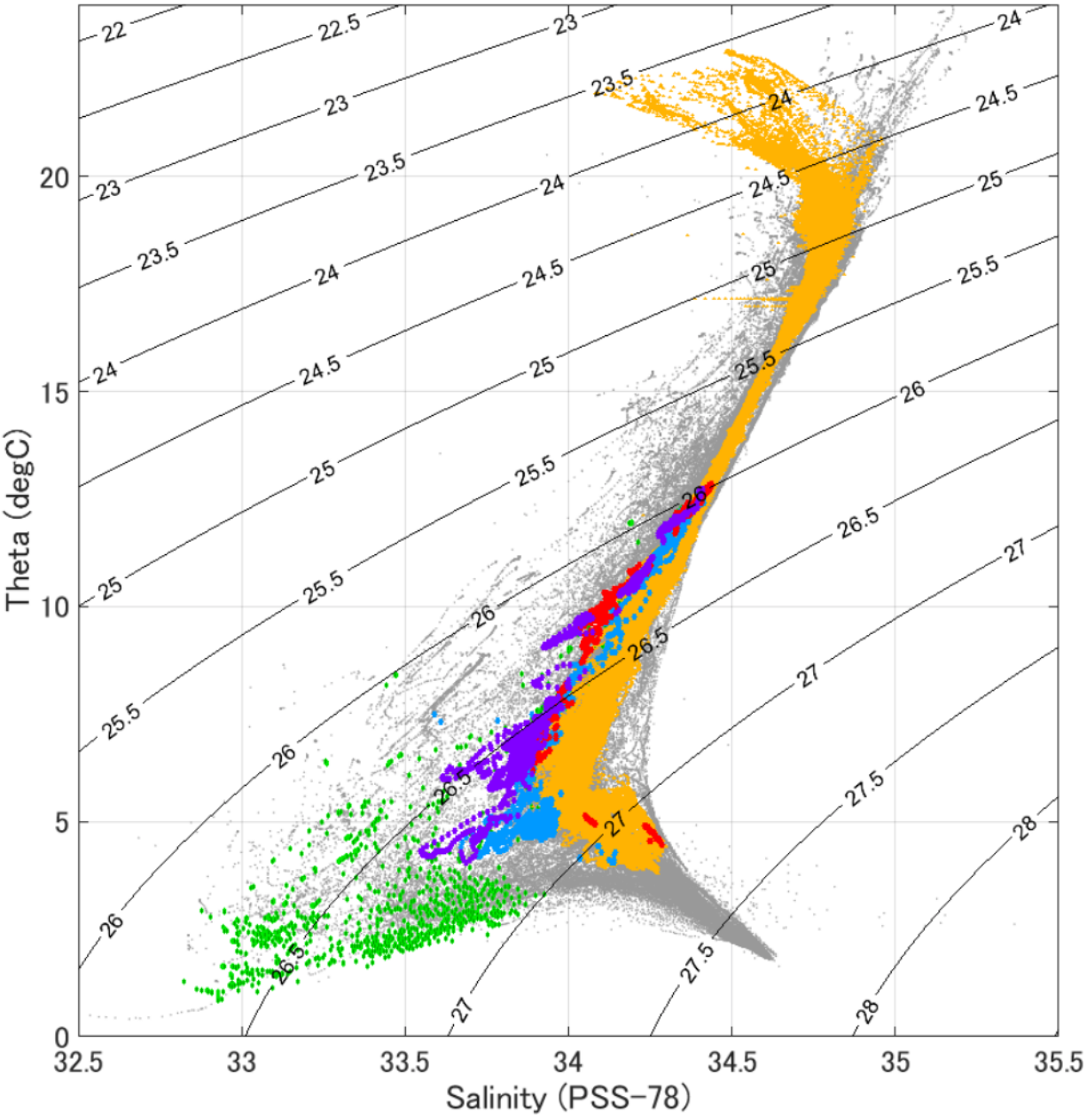

Figure 6

θ-S relations of seaglider data with over 3σ of negative salinity anomaly (blue circle), positive DO anomaly (red circles), and both (purple circles) during Apr.28-May 7, 2014. Orange dots are all seaglider data for Feb. 27-Jun. 21. Background gray dots show Argo data observed in 25-45°N, 140-160°E for Jan. 1-Apr. 30, 2014. Green dots are the same Argo data but observed in the upper subpolar region above 300 dbar at 41-45°N, 142-160°E.

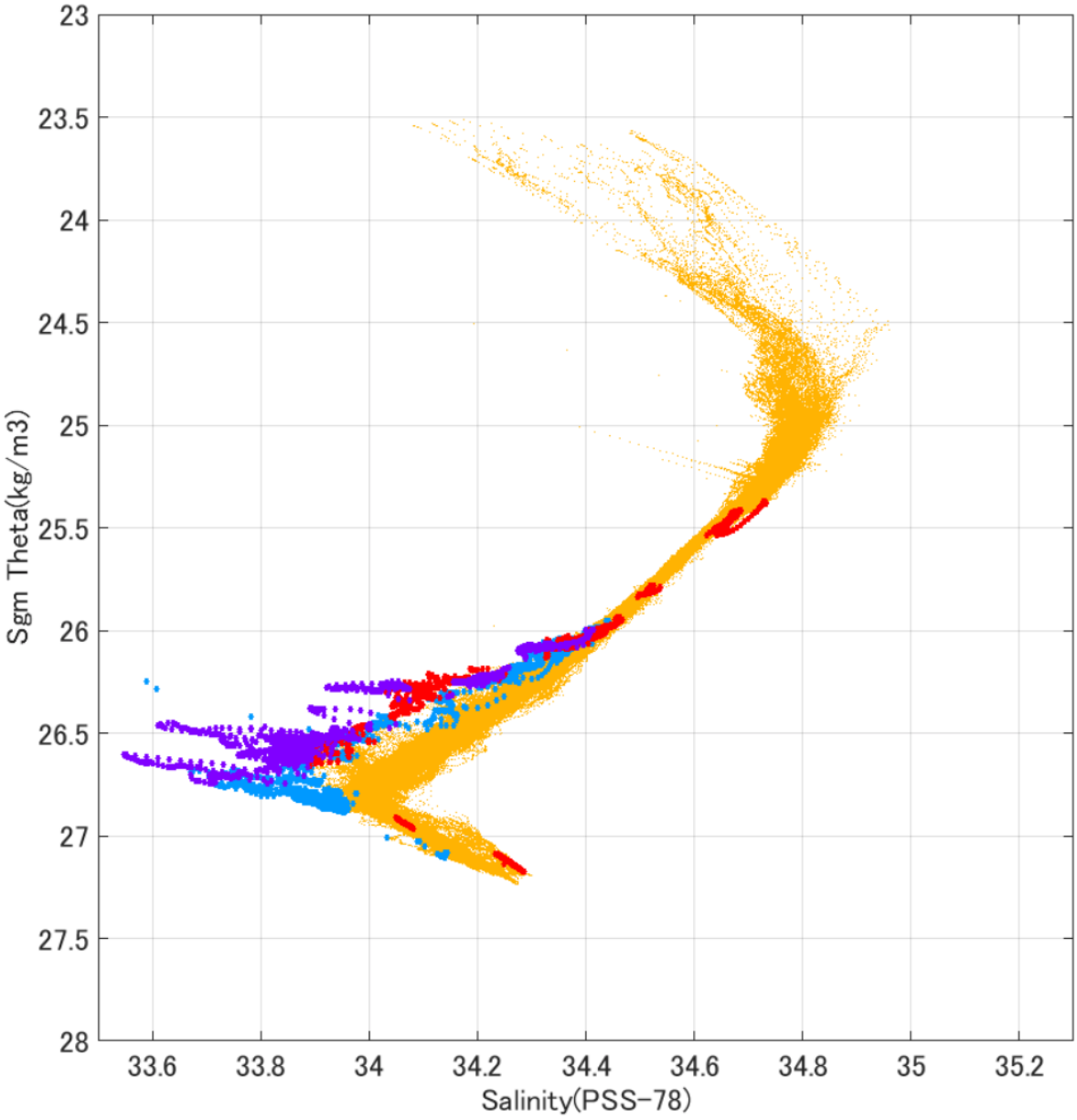

Figure 7

σθ-S diagram of Seaglider data, colored with over 3σ of negative salinity anomaly (blue circle), positive DO anomaly (red circles), and both (purple circle) below 400 dbar during Apr. 28-May 7. Orange dots are the other Seaglider data for whole observed period in Feb. 27-Jun. 21.

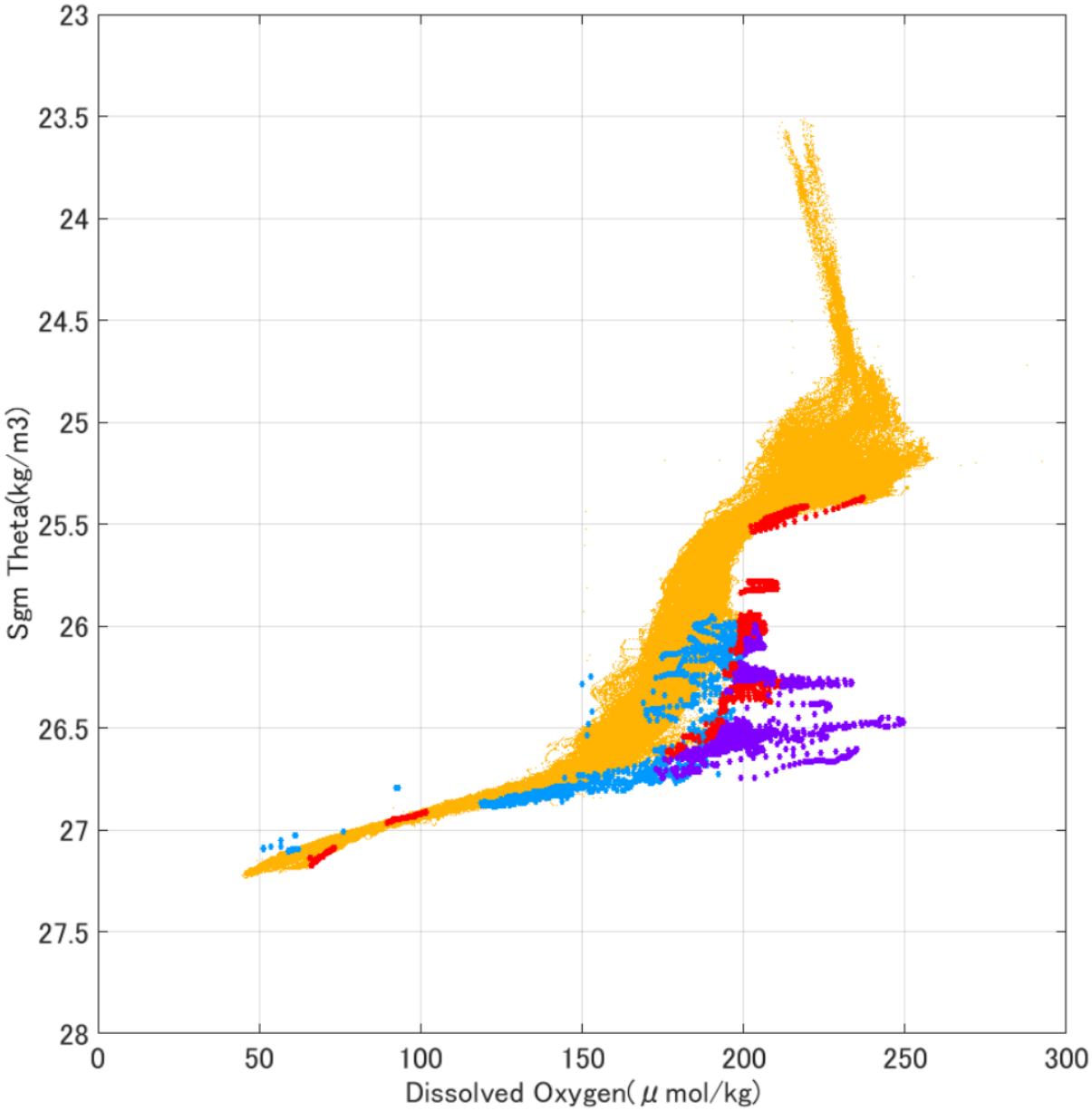

Figure 8

Same as Fig. 7 except for σθ-DO diagram of Seaglider data, colored with over 3σ of negative salinity anomaly (blue circle), positive DO anomaly (red circles), and both (purple circle).

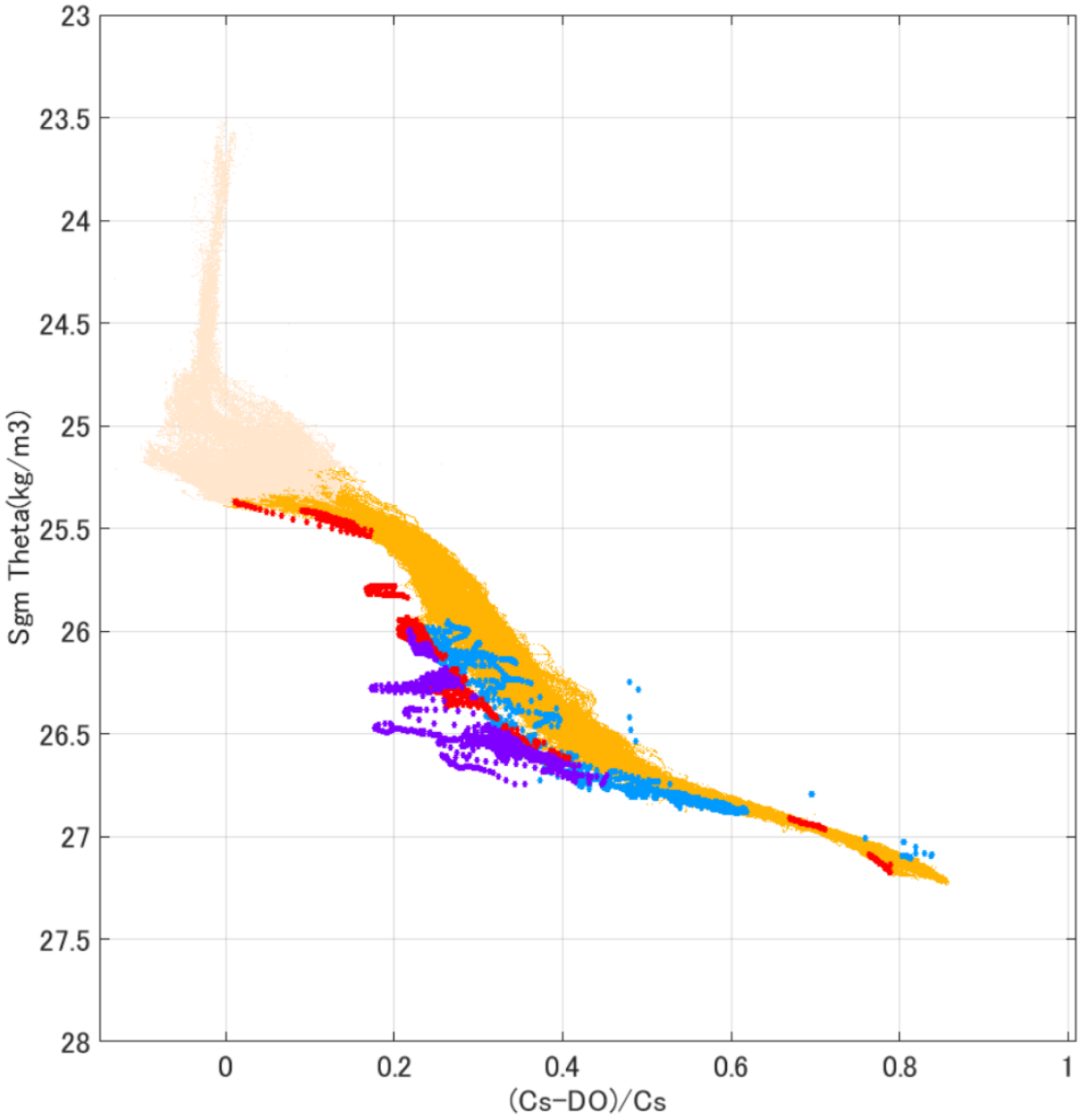

Figure 9

Same as Fig. 7 and 8 except for σθ-AOU/Cs Ratio diagram, colored with over 3σ of negative salinity anomaly (blue circle), and positive DO anomaly (red circles), and both (purple). The AOU is calculated by Cs-DO. Light orange indicates DO measurement in the euphotic zone.

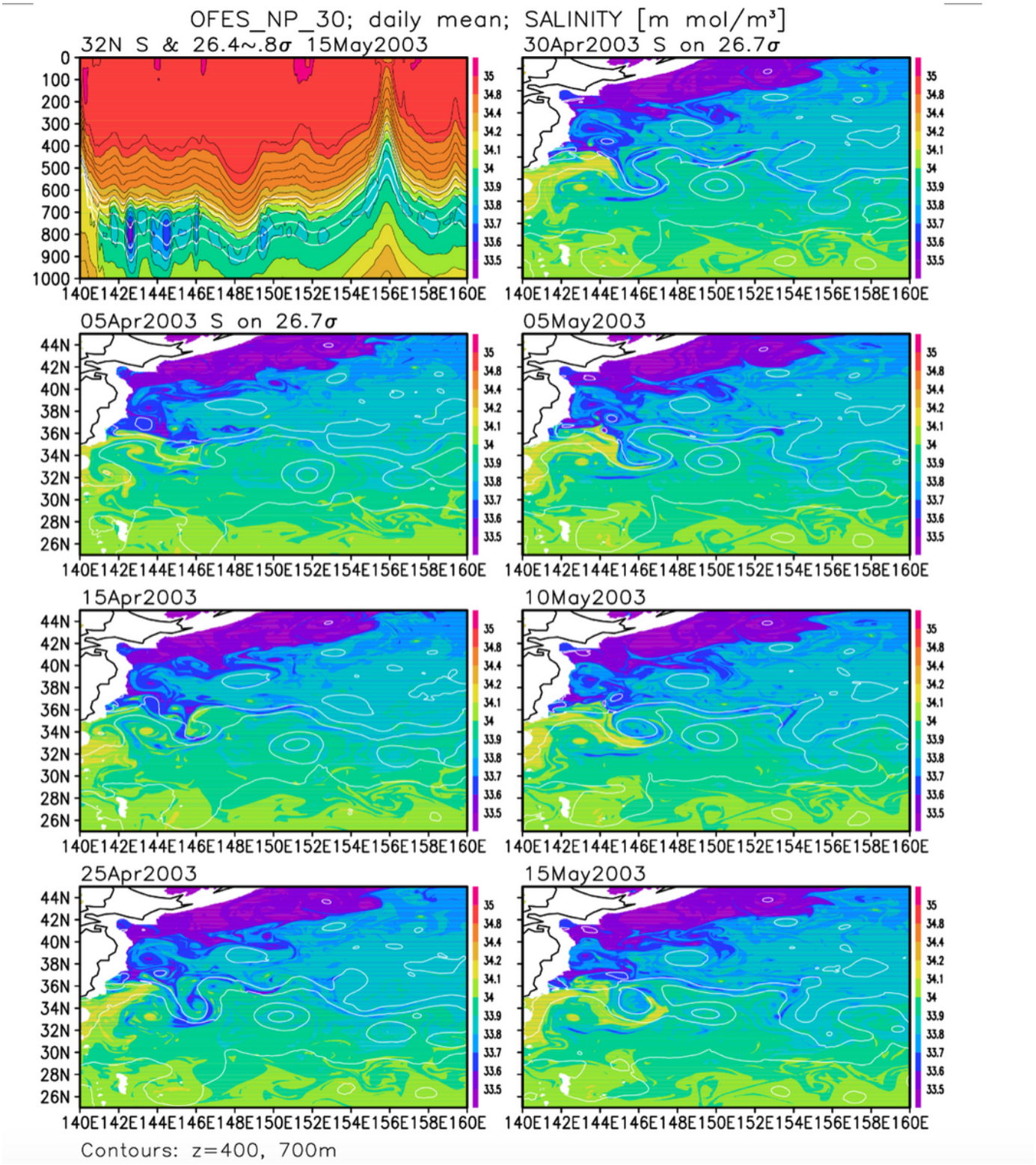

Figure 10

(Upper left) Zonal section of daily mean salinity along 32N on May 15, 2003 in the time of OFES. Contour intervals is 0.1 PSS-78. White contours show isopycnal depth at 26.4-26.8σθ. (2nd left to lower right) Salinity on 26.7 σθ surface in the western North Pacific (PSS-78) based on 1/30 high resolution OFES data. White color contour means 400m and 700m depths on 26.7σθ isopycnal surface. Each panel shows every 5 days from Apr. 5 (2nd left) to May 10 (lower right).

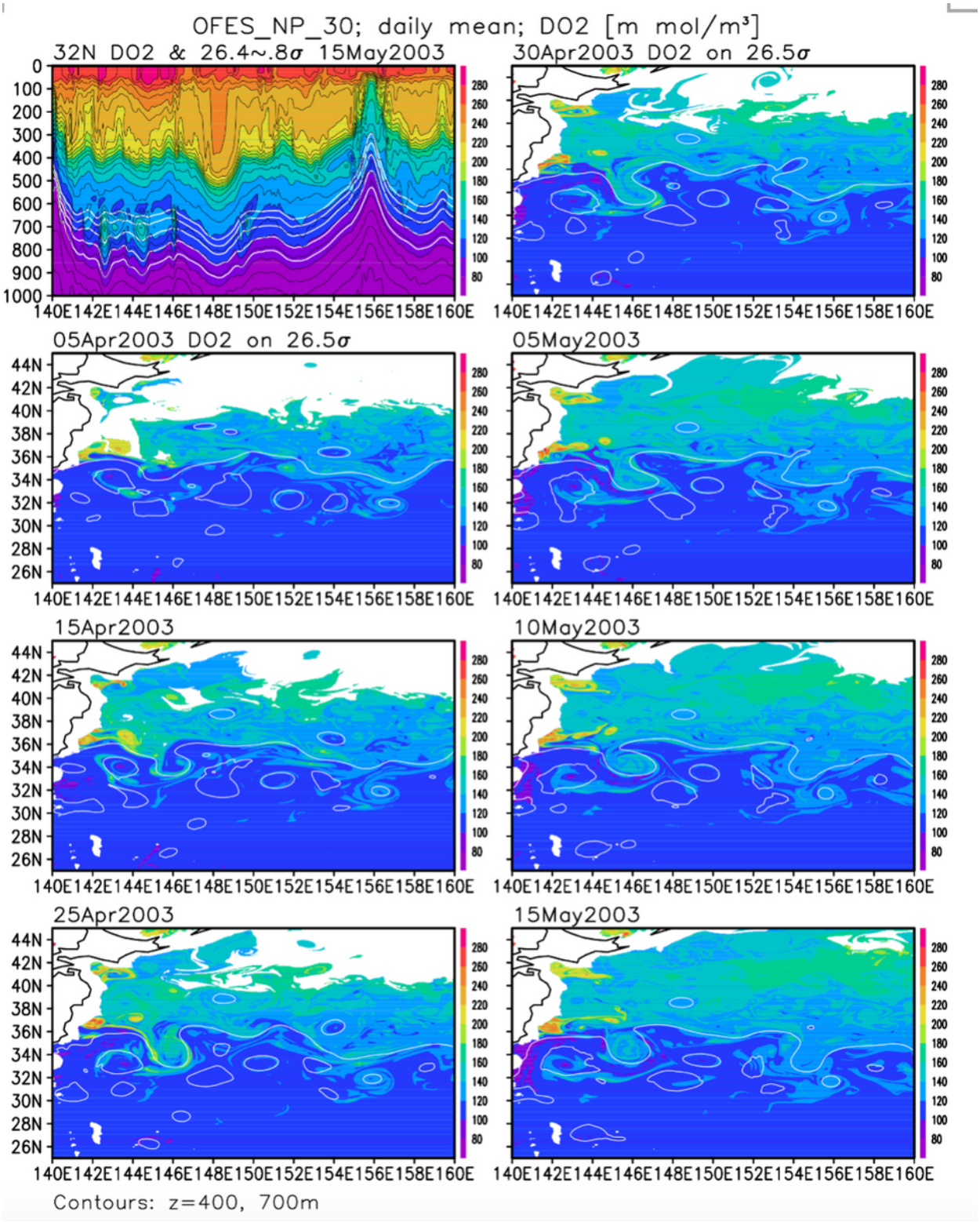

Figure 11

Same as Fig. 10 except for Dissolved oxygen (DO) concentration (unit: μmol kg-1) and DO distributions on 26.5 σθ surface.